 doi:10.20944/preprints202206.0245.v1

Article

MEMS Vibrometer for Structural Health Monitoring Using Guided Ultrasonic Waves

Jan Niklas Haus [1,*], Walter Lang [2], Thomas Roloff [3], Liv Rittmeier [3], Sarah Bornemann [2], Michael Sinapius [3] and Andreas Dietzel [1]

[1] Institute of Microtechnology, Technische Universität Braunschweig, 38124 Braunschweig, Germany; a.dietzel@tu-braunschweig.de
[2] Institute for Microsensors, Actuators and Systems, University of Bremen, 28359 Bremen, Germany; wlang@imsas.uni-bremen.de; sbornemann@imsas.uni-bremen.de
[3] Institute of Mechanics and Adaptronics, Technische Universität Braunschweig, 38106 Braunschweig, Germany; thomas.roloff@tu-braunschweig.de l.rittmeier@tu-braunschweig.de; m.sinapius@tu-braunschweig.de
* Correspondence: j.haus@tu-braunschweig.de; Tel. +49-531-391-9759

Abstract: Structural health monitoring of lightweight constructions made of composite materials can be performed using guided ultrasonic waves. If modern fiber metal laminates are used, this requires integrated sensors that can record the inner displacement oscillations caused by the propagating guided ultrasonic waves. Therefore, we have developed a robust MEMS vibrometer that can be integrated with structural and functional compliance. This vibrometer is directly sensitive to the high-frequency displacements from structure-borne ultrasound when excited between its first and second natural frequency. The vibrometer is mostly realized by processes earlier developed for a pressure sensor but with additional femtosecond laser ablation and wafer bonding. The piezoresistive transducer made from silicon is encapsulated between top and bottom glass lids. The natural frequencies are experimentally determined using an optical micro vibrometer setup. The vibrometer functionality and usability for structural health monitoring are demonstrated on a customized test rig by recording application-relevant guided ultrasonic wave packages with a central frequency of 100 kHz at a distance of 0.2 m from the exciting ultrasound transducer.

Keywords: MEMS vibrometer; Structural Health Monitoring (SHM); Guided Ultrasonic Waves (GUW); Fiber Metal Laminates (FML); wafer bonding

1. Introduction

In structural health monitoring (SHM) in fiber composites, guided ultrasonic waves (GUW) are suitable for damage detection [1]. Surface-mounted, usually piezoelectric, transducers are used to emit ultrasound bursts into the structure. The propagation of the GUW is then monitored by a sensor network to detect, localize and quantify structural damage, which locally changes the acoustic impedance leading to reflections and possibly to mode conversions [2]. Fiber metal laminates (FML) are being researched and partially already used in aerospace, as they combine the high specific strength of fiber composites with the ductile properties of metals. In FML, due to the high impedance differences between the metal layers and the layers of fiber-reinforced plastic, the wave propagation information is relevant to SHM mainly in the inner material layers. Therefore, sensor systems are required that can be embedded in the material with minimal retroactive effect on the propagation of GUW. Piezoelectric bending-mode sensors however typically cover at least half a wavelength of the ultrasound to efficiently detect GUW [2,3]. In addition, the acoustic properties of piezoceramics are poorly adapted to the laminate material, resulting in a discontinuity of the acoustic impedance. Inertial MEMS (Micro Electro-Mechanical System) sensors, in contrast, are based on excitation in form of displacements of the housing and can therefore be miniaturized to the technical limits. Moreover, glass as a typical MEMS

Preprints (www.preprints.org) | NOT PEER-REVIEWED | Posted: 17 June 2022 doi:10.20944/preprints202206.0245.v1

housing material is acoustically much better adapted to the polymer of FML [4].
However, typical MEMS accelerometers, such as those used for low frequency SHM in civil engineering structures, have a bandwidth of a few kHz, which is far below ultrasound. Examples are the Analog Devices ADXL 345 with 3200 Hz [5] or the ST AIS2IH with 1600 Hz [6]. While accelerometers are sensitive to accelerations at frequencies well below the resonance, seismometers become more sensitive for displacements at frequencies above the fundamental resonance frequency [7]. This makes the seismometer concept more suitable for the detection of GUW. Certainly, out-of-plane motions at ultrasound frequencies can be also be detected with optical vibrometers such as the laser Doppler vibrometer (LDV). But unlike these optical techniques, which only have access to the visible surface of a structure, a MEMS sensor can be embedded to capture information from inside a structure. Therefore, the concept of a MEMS seismometer as embeddable vibrometer for the detection of GUW was recently proposed by the authors [4]. A GUW detection scheme based on this concept requires a sealed MEMS vibrometer that can be integrated into the layered structure of FML without perturbing the propagating GUW. This article presents such a concept.

2. The concept of MEMS vibrometer response

Inertial sensors detect displacements of a spring-loaded mass m relative to the sensor base $y(t)$ as a function of the external mechanical stimulus in the form of displacements of the base $x(t)$, as illustrated in Figure 1.

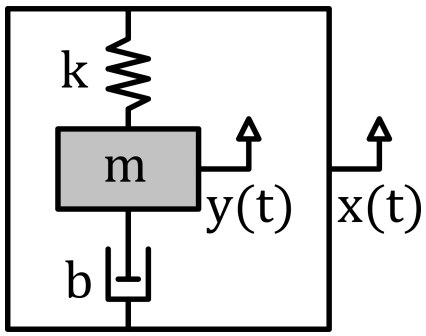

Figure 1. Schematic illustrating the inertial sensor concept [8]

The well-known governing equation (1) is

$$m \cdot \frac{d^2x(t)}{dt^2} = m \cdot \frac{d^2y(t)}{dt^2} + b \cdot \frac{dy(t)}{dt} + k \cdot y(t), \tag{1}$$

where m represents the mass, k the spring constant and b the damping. Such a system is characterized by the natural frequency ω_0 (2)

$$\omega_0 = \sqrt{\frac{k}{m}}. \tag{2}$$

This allows the complex frequency response to an acceleration stimulus G_{accel} to be given by Equation (3)

$$G_{accel}(i\omega) = \frac{\omega^2}{(\omega^2 - \omega_0^2) + \omega\frac{b}{m}} \cdot e^{-i\phi}, \phi = \tan^{-1}\left(\frac{b}{m} \cdot \frac{\omega}{\omega_0^2 - \omega^2}\right) \tag{3}$$

and the frequency response for a displacement stimulus G_{displ} is given as (4)

$$G_{accel}(i\omega) = -\omega^2 \cdot G_{displ}(i\omega) \tag{4}$$

.

Preprints (www.preprints.org) | NOT PEER-REVIEWED | Posted: 17 June 2022 doi:10.20944/preprints202206.0245.v1

In the quasi-static frequency range, where $\omega \ll \omega_0$, the sensors sensitivity to acceleration is given as $|G_{accel}| \approx \frac{1}{\omega_0^2}$ and the sensitivity to displacement as $|G_{displ}| = \omega^2 \cdot |G_{accel}| \approx 0$ (cf. Figure 2). For the case of quasi-free excitation, i.e. where $\omega \gg \omega_0$, sensitivities are given as $|G_{accel}| \approx \frac{1}{\omega^2} \approx 0$ and $|G_{displ}| = \omega^2 \cdot |G_{accel}| \approx 1$. As a consequence, the spring-loaded mass acts as an acceleration sensor for $\omega \ll \omega_0$ and as a displacement sensor for $\omega \gg \omega_0$.

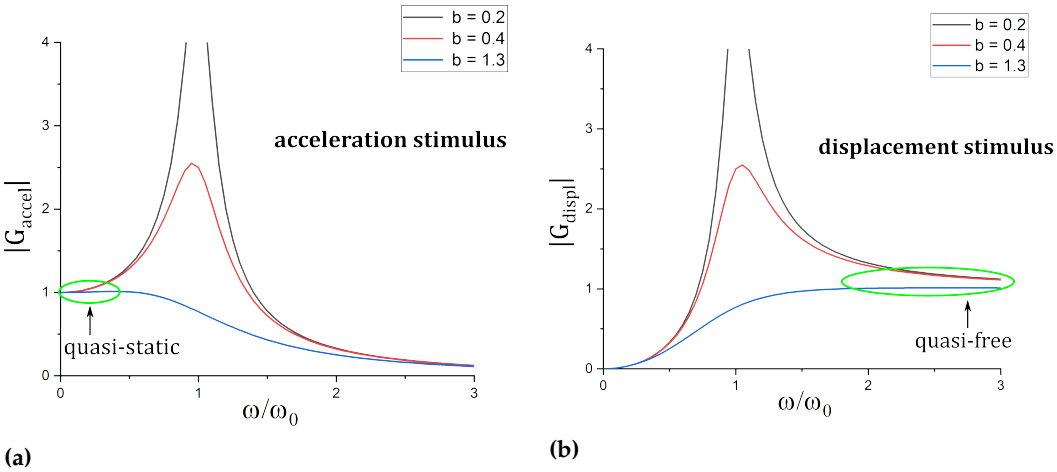

Figure 2. Frequency-dependent sensitivity to acceleration $|G_{accel}|$ **(a)** and sensitivity to displacement $|G_{displ}|$ **(b)**. The colors indicate different levels of damping.

In the case of an LDV, the displacement must be determined from the measured vibration velocity, i.e by integration. Any other device, which is also able to record the local vibrations with sufficient temporal resolution, can be referred to as a vibrometer. Here, a MEMS vibrometer with a micro cantilever as a key element shall be embedded in the FML structure to directly record the local displacements forced by the propagating GUW.
Due to the micro cantilever's continuous geometry, it behaves more complex than the model of a simple spring-mass damper system. In addition to ω_0, higher natural frequencies, each corresponding to a bending or torsion mode, appear. For the operation as a vibrometer, the detectable frequencies must be in between the lowest eigenfrequency ω_0 and the second natural frequency of the cantilever. The bending eigenfrequencies ω_i of a cantilever are obtained from the zeros of Equation (5) [9–11]

$$\cos \lambda_i \cdot \cosh \lambda_i = -1 \tag{5}$$

and Equation (6)

$$\omega_i = \lambda_i^2 \cdot \sqrt{\frac{E \cdot h^2}{12 \cdot \rho \cdot L^4}}. \tag{6}$$

Taking the geometry for the laser cut cantilever ($L = 540\,\mu m$, $t = 10\,\mu m$) and the material properties of silicon ($E_{<100>} = 165.6 \times 10^9\,N\,m^{-2}$, density $\rho = 2330\,kg\,m^{-3}$) the bending eigenfrequencies are predicted as

$$f_1 = 46.6\,kHz; f_2 = 292.2\,kHz; f_3 = 818.0\,kHz; f_4 = 1.60\,MHz.$$

These natural frequencies are higher than the actual natural frequencies of the sensor because the assumed boundary condition of a fixed clamping is not exactly correct.

3. Materials and Methods

3.1. Fabrication

The MEMS vibrometer fabrication using most of the process steps previously applied for a cavity-in-glass pressure sensor [12] is illustrated in Figure 3. A 200 µm-thick borosil-

Preprints (www.preprints.org) | NOT PEER-REVIEWED | Posted: 17 June 2022 doi:10.20944/preprints202206.0245.v1

icate glass wafer with hydrofluoric acid (HF)-etched cavities (a.) and femtosecond laser ($\lambda = 1030\,\mathrm{nm}$) made through holes (b.) and the device layer of silicon on insulator (SOI) wafer which is boron-doped (c.) with a scheme that will later yield a Wheatstone bridge are anodically bonded (d.). Magnetron sputtering of chromium and gold, and successive copper electroplating (e.) yield through-glass vias from the silicon Wheatstone circuit to a solderable chip-scale package, providing mechanical and electrical connection to a printed circuit board (PCB) substrate. The SOI's device layer forms a highly consistent 10 µm-thick membrane after removing the handle layer by KOH etching (f.). In order to create the micro cantilever, the membrane is modified on chip level by femtosecond laser ablation. A contour is cut (g.) into the membrane, thereby creating a cantilever with approx. measures of $540 \times 220 \times 10\ \mu\mathrm{m}^3$, while leaving the electrical circuit (as used for the pressure sensor design) intact. The piezoresistive path that senses the cantilever deflection is connected with complementary resistors to form a Wheatstone quarter bridge, as depicted in Figure 4a. To encapsulate the micro cantilever, a second borosilicate wafer with HF-etched cavities (a.) is anodically bonded (h.) to the silicon device layer. The 4-inch wafer is diced into 552 MEMS vibrometer chips. Finally, the obtained MEMS vibrometer chip-scale package is mounted to a 25 µm-thin flexible polyimide PCB (see Figure 4b).

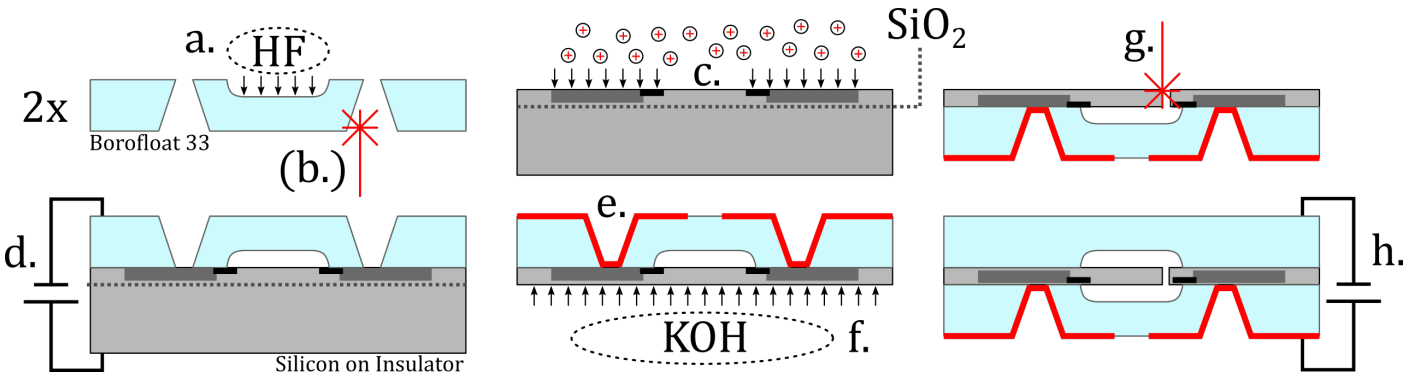

Figure 3. Illustration of the MEMS vibrometer microfabrication: a.) HF cavity etching into borofloat wafer; b.) through-glass vias by fs laser ablation; c.) local boron doping of the SOI device layer; d.) anodic bonding of SOI and borofloat wafers; e.) metallization by Cr+Au magnetron sputtering and successive Cu electroplating; f.) removing handle layer by KOH etching; g.) fs laser cutting cantilever into membrane; h.) encapsulation by anodically bonding a glass lid.

Preprints (www.preprints.org) | NOT PEER-REVIEWED | Posted: 17 June 2022 doi:10.20944/preprints202206.0245.v1

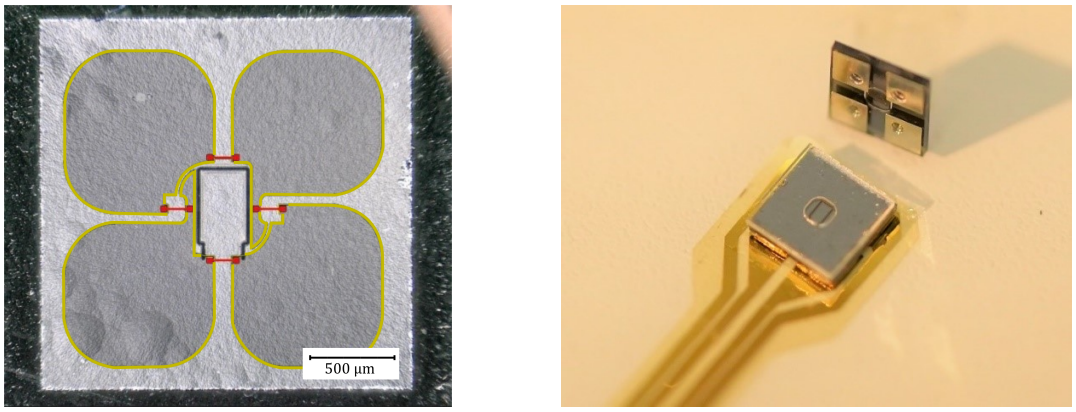

(a) **(b)**

Figure 4. a) Microscopic image of the chip surface after step (g.) showing the femtosecond laser cuts in the silicon membrane and the Wheatstone bridge doping scheme. Dark gray areas marked by yellow frames indicate the highly boron doped silicon wiring; the four much smaller piezoresistive tracks with weaker doping are marked in red color. **b)** MEMS vibrometers with $2\,mm \times 2\,mm$ lateral dimensions and a thickness of 410 µm. One is mounted onto polyimide PCB substrate by reflow soldering.

3.2. Experimental modal analysis of the MEMS

To gain a better understanding of the sensor's dynamic behavior, the natural frequencies and the corresponding modal shapes of the inherent micro cantilever are experimentally determined. The test setup (cf. Figure 5) comprises a scanning laser vibrometer that integrates a confocal microscope and a shaker stage for the high-frequency out-of-plane excitation with nanometer-scale amplitudes (PicoScale Vibrometer, SmarAct Metrology). The MEMS vibrometer chip is mechanically coupled to the shaker stage using vacuum grease. After imaging the region of interest, single point vibrometry is performed at a corner of the cantilever tip (cf. Figure 8b), allowing to monitor bending and torsional modes. A frequency sweep with constant amplitude is used as excitation signal such that after Fourier transformation, it is possible to correlate the induced displacement to excitation frequency (Figure 10a). For the imaging of the cantilever vibrational modes, the sample is excited with a harmonic sinusoid. Then, the measurement laser is raster-scanned over the sample and the obtained displacement data is fed into the internal digital lock-in amplifier, so that for each pixel the amplitude and phase of the vibration can be determined. With this data, the cantilever mode shapes can be directly observed, as presented in Figure 9.

Preprints (www.preprints.org) | NOT PEER-REVIEWED | Posted: 17 June 2022 doi:10.20944/preprints202206.0245.v1

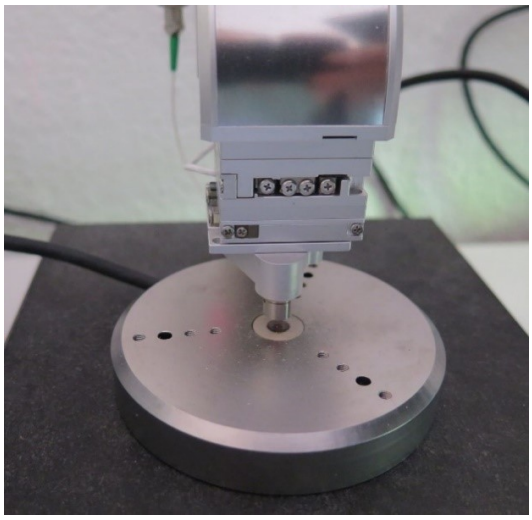

Figure 5. Measurement setup: the vibrometer head from the PicoScale Vibrometer is raster-scanned over the sample, fixated onto the shaker stage for the dynamic characterization of the MEMS vibrometer chip.

3.3. Set-up for dynamic sensor signal response characterization

The test bed shown in Figure 6 allows to characterize the electrical sensor response to ultrasonic structural displacements. A piezoelectric transducer (PRYY+0226, PI Ceramics) with a diameter of 10 mm, a thickness of 0.5 mm and with wrap-around electrodes is soldered to a PCB substrate, yielding a simplified shaker stage. On top of it, the flexible polyimide PCB on which the chip scale MEMS vibrometer is mounted is adhesively bonded. Using a function generator and a high-frequency voltage amplifier (PD200, PiezoDrive), the shaker stage can be excited with arbitrary signals. Simultaneously, the output voltage of the MEMS vibrometer is recorded using a high-frequency Wheatstone bridge amplifier (DEWE 30-40, DEWETRON). As a reference, the spot of an LDV (PSV 400, Polytec) is directed to the chip transducer, directly next to the MEMS vibrometer chip. Using a sweep excitation from 0 – 500 kHz, the MEMS vibrometer's transfer behavior can be derived. To demonstrate the MEMS vibrometer's ability to acquire ultrasound packages, as used for the SHM applications, the piezoelectric transducer is excited with short bursts with a center frequency of 100 kHz (cf. Figure 11).

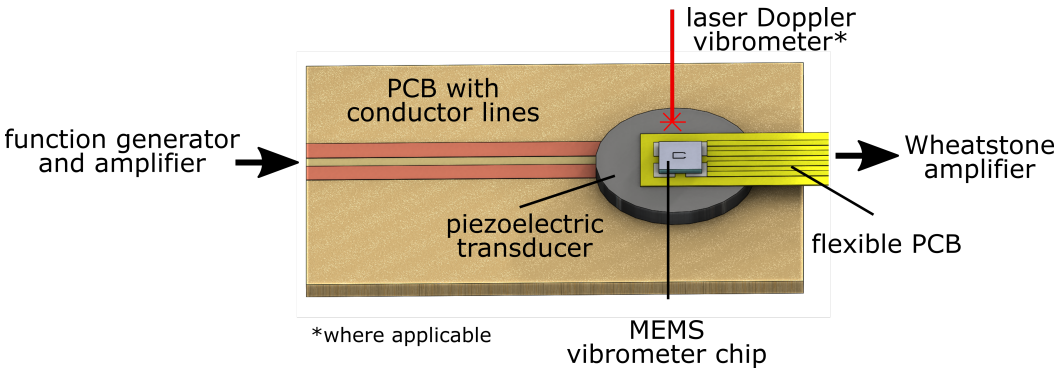

Figure 6. 3D sketch of the test bed for the dynamic sensor response characterization.

3.4. GUW setup

The MEMS vibrometer is mounted onto a 0.5 m long FML strip to demonstrate the functionality of sensing GUWs. The strip is made out of carbon fiber reinforced polymer (CFRP) and steel with the stacking sequence $[\text{steel}/0_4/\text{steel}/0_2]_S$ and a nominal thickness of 2.02 mm. Ultrasonic, hanning-windowed sinusoidal bursts are excited at one edge using a rectangular piezoceramic with a thickness of 0.2 mm, cf. Figure 7. The thereby excited

Preprints (www.preprints.org) | NOT PEER-REVIEWED | Posted: 17 June 2022 doi:10.20944/preprints202206.0245.v1

waves propagate through the wave guide. In 0.2 m of distance from the excited edge, the MEMS vibrometer is mounted. In addition to the electrical response, the out-of-plane velocity is measured by the LDV measuring directly next to the sensor.

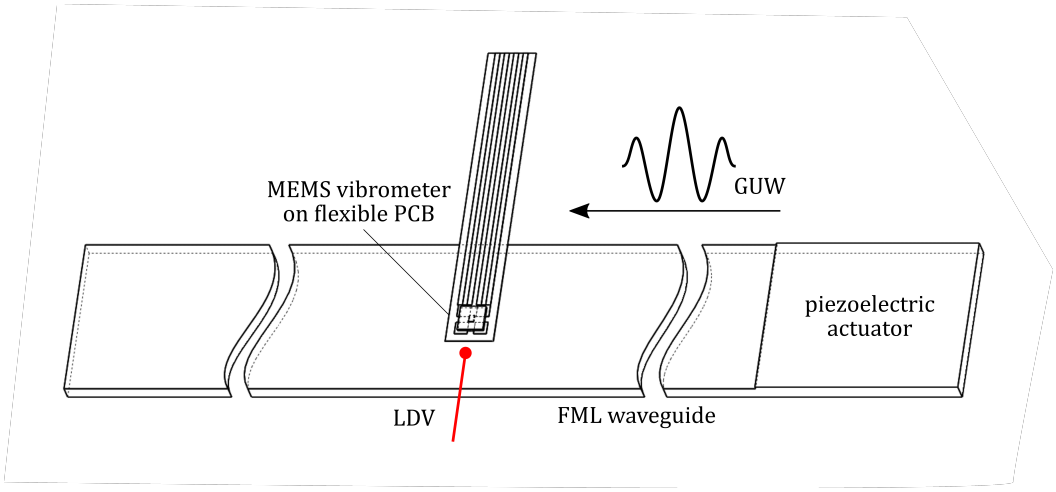

Figure 7. Test setup for GUW sensing experiments: FML waveguide with surface-bonded piezoceramic actuator, applied MEMS vibrometer and reference LDV measurement in a distance of 0.2 m from excitation.

4. Results

4.1. Modal analysis of the micro cantilever

Figure 8a shows the amplitude response of the cantilever up to 500 kHz as obtained with the SmarAct PICOSCALE vibrometer at the indicated (red mark) location in Figure 8b. Three major resonances appear at 42 kHz, 162 kHz and 281 kHz. Parasitic peaks at 99 kHz, 112 kHz, 393 kHz and 473 kHz originate from the electronics of the vibrometer.

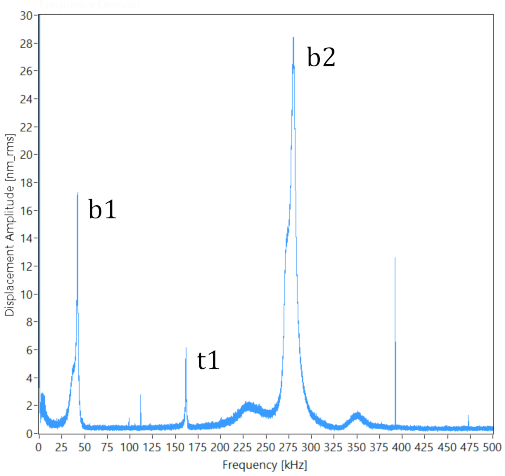

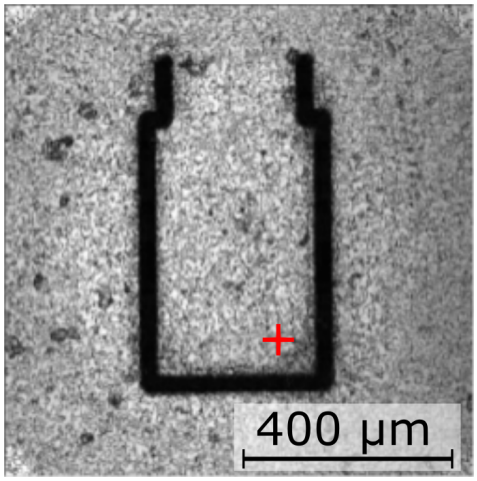

(a) **(b)**

Figure 8. a) Vibrational response of the micro cantilever measured at the location indicated by the red mark in the microscopy image **b).** Peaks b1, b2 and t1 denote bending and torsional modes.

The images obtained with the micro vibrometer (Figure 9) show the shapes of bending and torsion modes up to a frequency of 500 kHz. The obtained resonances are in good agreement with the analytical predictions.

4.2. Dynamic MEMS vibrometer response

Figure 10a shows the electrical signal amplitude spectrum of the MEMS vibrometer between 0 and 500 kHz as obtained on the piezoceramic shaker stage (Figure 6). Narrow

Preprints (www.preprints.org) | NOT PEER-REVIEWED | Posted: 17 June 2022 doi:10.20944/preprints202206.0245.v1

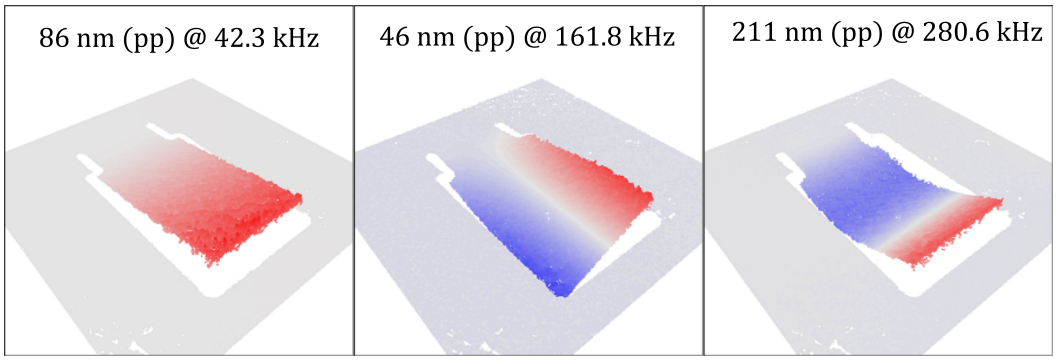

Figure 9. Representation of the bending (left, b1 and right, b2) and torsional (center, t1) modes recorded with the laser scanning vibrometer. Red and blue coloring represents the normalized deflection. The amplitudes shown correspond to the peak-to-peak values.

resonances can be recognized around 50 kHz, 180 kHz and 300 kHz which fit quite well to both the previously calculated and measured mechanical resonances of the micro cantilever. In addition, some broader peaks are found in the spectrum that are influenced by GUW reflections and resonance phenomena in the measurement setup. To verify this, the complex velocity spectrum, as obtained by the LDV between 0 and 500 kHz, is multiplied with $j\omega$ to obtain the displacement spectrum of the shaker stage the MEMS vibrometer is applied on. Figure 10b depicts the amplitude spectrum of the shaker stage's displacement. Even though the LDV spot could not be exactly placed on the MEMS chip frame, this measurement can be regarded as approximately representing the frequency characteristics of the sensor's mechanical excitation. As expected, the LDV spectrum reveals a dynamic behavior of the shaker stage that appears in the MEMS signal as well, e.g. the broad peak at approx. 220 kHz. However, the sharp peaks in the sensor signal do not appear in the shaker stage's displacement spectrum so that they can be clearly identified as the sensor's resonances.

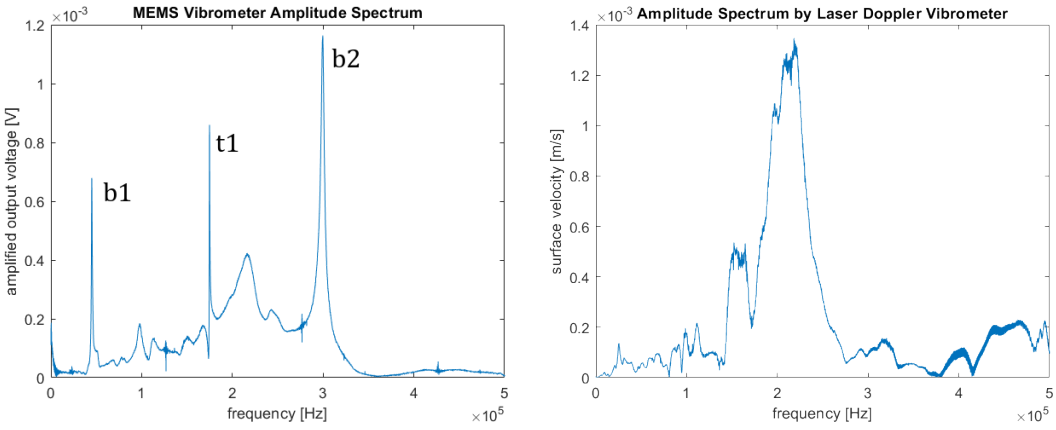

(a) **(b)**

Figure 10. a) Frequency response of the MEMS vibrometer chip as obtained by the setup shown in Figure 6. Bending- (b1, b2) and torsional modes (t1) are indicated. **b)** displacement amplitude as obtained by the LDV measurement

Using the same setup, the piezoelectric transducer was excited with five-cyclic, Hanning-windowed 100 kHz sinusoidal bursts, as presented in Figure 11, top. This ultrasonic signal is typically used for SHM. Figures 11, middle, depicts the thereby stimulated signals from the LDV; the MEMS vibrometer signals are given in Figure 11, bottom.

The excitation wave package is reflected at the edge of the transducer, leading to superposition of the initial signals and signals from reflections. The LDV measurements represent the resulting out-of-plane velocities picked up at the transducer surface close to the chip. The MEMS vibrometer shows a mixed signal: At first, the excitation signal

Preprints (www.preprints.org) | NOT PEER-REVIEWED | Posted: 17 June 2022 doi:10.20944/preprints202206.0245.v1

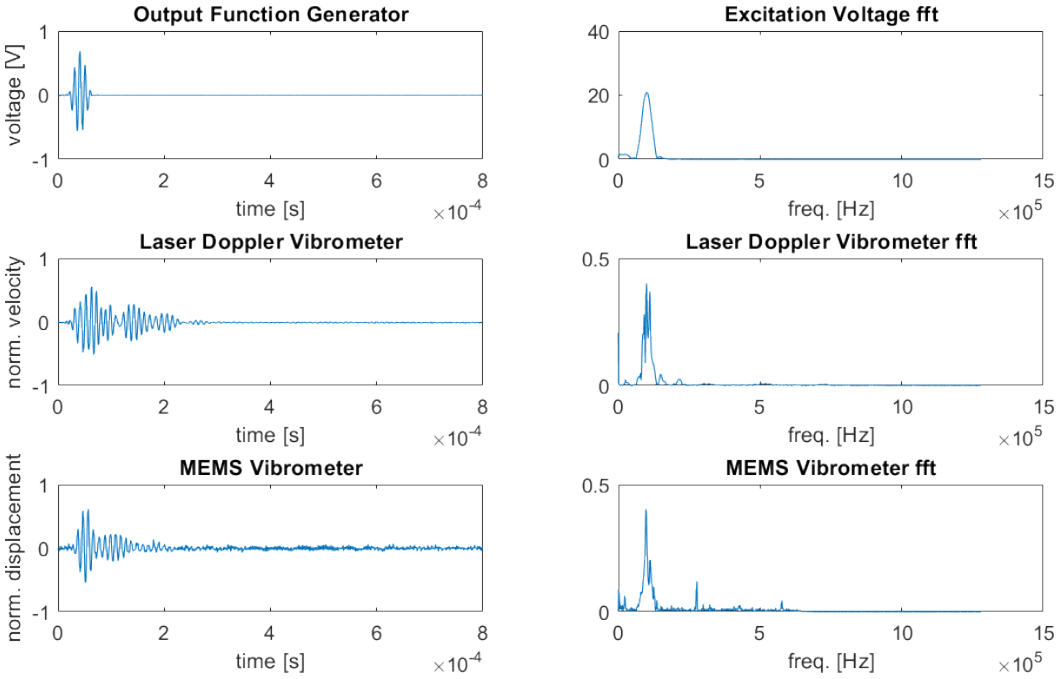

Figure 11. Excitation and vibrometer (MEMS and LDV) response signals, as obtained by the setup shown in Figure 6. Ultrasonic bursts, as they are used for SHM were used as a stimulus.

electrically couples into the sensor signal, after the electrical stimulus has ended, the sensor signal represents the out-of-plane displacement of the MEMS chip.

4.3. Detection of GUW

To demonstrate the MEMS vibrometer's ability to acquire GUW, ultrasonic sine bursts are excited into an FML waveguide. These are then recorded by the MEMS vibrometer and an LDV at the approx. same position but on the waveguide. Unlike the experimental setup in Figure 6, this configuration in Figure 7 allows the ultrasonic wave package to propagate through the FML waveguide before it is picked up by the LDV and the MEMS vibrometer. In Figure 12, the signals of excitation (top), LDV (middle) and MEMS vibrometer (bottom) are displayed. The LDV signal depicts a first wave package at $t \approx 70\,\mu s$ and a second one at $t \approx 180\,\mu s$. Considering the excitation of the GUW at $t \approx 50\,\mu s$ and the distance traveled to be 0.2 m this results in group velocities of approx. $6650\,m\,s^{-1}$ and $1450\,m\,s^{-1}$ for the first and second wave package, respectively. This is in good agreement with the theoretically expected group velocities for the S_0- and A_0-mode, respectively. Another indicator supporting this conclusion is the signal amplitude. The first measured wave package, corresponding to the S_0-mode, has a lower amplitude than the second one. The LDV measures the structural velocity in laser direction which is nearly perpendicular to the specimen's surface resulting in a higher sensitivity for out-of-plane vibrations. In this frequency range, the A_0-mode has a higher out-of-plane proportion than the S_0-mode.
The MEMS vibrometer is equally capable of detecting two wave packages. However, the first one is due to an electrical cross-talk, meaning that the electrical excitation signal directly couples into the MEMS signal with no delay and covers a eventually occurring S_0 wave package. This should be avoidable with better electrical shielding. The second wave package is detected at $t \approx 180\,\mu s$. This is again the A_0-mode with a higher out-of-plane component. This measurement is in good agreement with the working principle of the MEMS vibrometer as it is designed to be sensitive in the out-of-plane direction.
These measurements validate the concept of a MEMS vibrometer for detecting the out-of-plane component of GUW. At frequencies lower than the first resonance, a sensitivity to acceleration exists, but more importantly a sensitivity to displacements can be concluded

Preprints (www.preprints.org) | NOT PEER-REVIEWED | Posted: 17 June 2022 doi:10.20944/preprints202206.0245.v1

between the first bending- and the first torsional resonance and therefore between 40 kHz and 160 kHz .

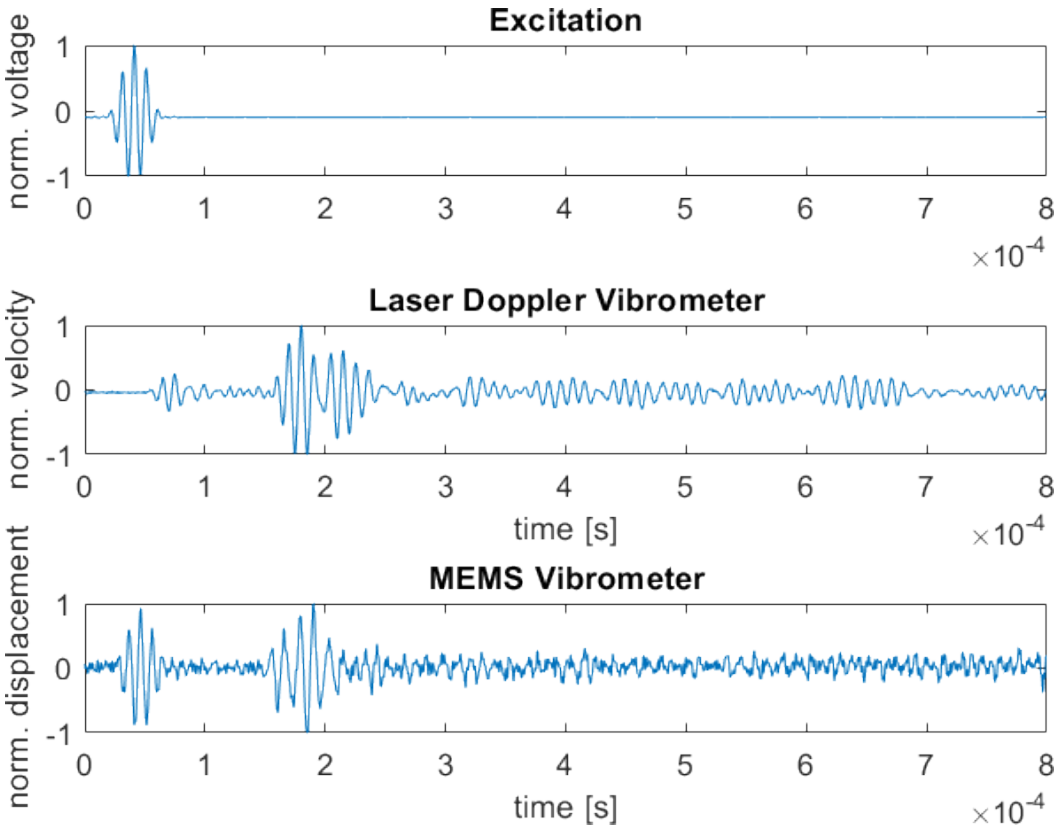

Figure 12. Comparison of signals of GUW. Top: Excitation signal (output of function generator). Middle: Signal acquired with the LDV with S_0 wave package at $t \approx 70\,\mu s$ and A_0 wave package at $t \approx 180\,\mu s$. Bottom: Signal of the MEMS vibrometer with electrical cross-talk at $t \approx 50\,\mu s$ and A_0 wave package at $t \approx 180\,\mu s$.

5. Discussion

A MEMS vibrometer is presented that can be embedded in the layered structure of FML and capture information from inside the structure without disturbing the propagating GUW. The MEMS vibrometer is based on a mechanical spring loaded mass oscillator that can sense dynamic displacement fields of structure-born ultrasound beyond its first natural frequency. The dynamic behavior of the spring mass system was investigated by means of micro-LSV and eigenmodes could be identified. Between the first bending- and the first torsional resonance, i.e. between 40 kHz and 160 kHz, a sensitivity to displacement was confirmed. The sensor was therefore ideally suited for receiving GUW bursts with a center frequency of 100 kHz. We demonstrated this capability using a GUW setup with an FML strip as wave guide. The MEMS vibrometer could record GUW that had traveled over 0.2 m distance to their excitation. The signals were in good agreement with those obtained with an LDV positioned in the proximity of the MEMS vibrometer. The presented MEMS vibrometer is encapsulated in a glass chip package and can be embedded into a composite structure in a next step to capture ultrasonic displacement fields of e.g. the inner material layers. Due to its non-isotropic sensitivity, out-of-plane displacements can be selectively recorded and GUW mode selectivity can be achieved even for a single point of interest. Future work will investigate MEMS design with improved sensitivity and bandwidth using a tailored MEMS characterization environment [13]. Further, sensor damping adjustment will be made possible by entrapping gas of defined pressure inside the sensor cavity. Preliminary embedding experiments could already demonstrate the successful integration of MEMS vibrometers into both glass laminate aluminum reinforced epoxy (GLARE) and CFRP-steel plates. In future work, an integrable sensor data acquisition node [14], will be used to wirelessly power the vibrometer and read its GUW signals.

 doi:10.20944/preprints202206.0245.v1

Author Contributions: Conceptualization, Jan Niklas Haus, Liv Rittmeier, Michael Sinapius and Andreas Dietzel; Data curation, Jan Niklas Haus, Thomas Roloff, Liv Rittmeier and Sarah Bornemann; Formal analysis, Jan Niklas Haus, Walter Lang, Thomas Roloff, Liv Rittmeier and Andreas Dietzel; Funding acquisition, Michael Sinapius and Andreas Dietzel; Investigation, Jan Niklas Haus, Thomas Roloff, Liv Rittmeier and Sarah Bornemann; Methodology, Jan Niklas Haus, Thomas Roloff, Liv Rittmeier, Sarah Bornemann and Andreas Dietzel; Project administration, Michael Sinapius and Andreas Dietzel; Supervision, Michael Sinapius and Andreas Dietzel; Validation, Thomas Roloff; Visualization, Jan Niklas Haus; Writing – original draft, Jan Niklas Haus, Walter Lang and Andreas Dietzel; Writing – review & editing, Walter Lang, Thomas Roloff, Sarah Bornemann, Michael Sinapius and Andreas Dietzel.

Funding: The authors expressively acknowledge the financial support of the research work on this article within the Research Unit 3022 "Ultrasonic Monitoring of Fibre Metal Laminates Using Integrated Sensors" by the German Research Foundation (Deutsche Forschungsgemeinschaft (DFG)), Project-ID 418311604.

Informed Consent Statement: Not applicable

Acknowledgments:
The authors would like to thank Semjon Köhnke, Michael Lherbette and Iwan Schaap, representing SmarAct GmbH for the kind supply with the experimental modal analysis, and the metrological background in this field. Further, the authors would like to express their gratitude to Bettina Thürmann, Jonas Himmelstoß and Michael Wiegandt for their continuous efforts in microfabrication and tool-manufacturing.

Conflicts of Interest: The authors declare no conflict of interest.

References

1. Giurgiutiu, V. *Structural health monitoring with piezoelectric wafer active sensors*; Academic Press/Elsevier: Amsterdam, 2008.
2. Lammering, R.; Gabbert, U.; Sinapius, M.; Schuster, T.; Wierach, P. *Lamb-wave based structural health monitoring in polymer composites*; Springer, 2017.
3. Lissenden, C.; Liu, Y.; Choi, G.; Yao, X. Effect of localized microstructure evolution on higher harmonic generation of guided waves. *Journal of Nondestructive Evaluation* **2014**, *33*, 178–186.
4. Haus, J.N.; Rittmeier, L.; Roloff, T.; Mikhaylenko, A.; Bornemann, S.; Sinapius, M.; Rauter, N.; Lang, W.; Dietzel, A. Micro-Oscillator as Integrable Sensor for Structure-Borne Ultrasound. *Engineering Proceedings* **2021**, *10*, 81.
5. Analog Devices. *3-Axis, ±2 g/±4 g/±8 g/±16 g Digital Accelerometer*, 2022. Rev. G; https://www.analog.com/media/en/technical-documentation/data-sheets/ADXL345.pdf; accessed: 2022-06-14.
6. STMicroelectronics. *MEMS digital output motion sensor: High-performance 3-axis accelerometer for automobile applications*, 2021. Rev. 4; https://www.st.com/resource/en/datasheet/ais2ih.pdf; accessed: 2022-06-14.
7. Younis, M.I. *MEMS linear and nonlinear statics and dynamics*; Vol. 20, Springer Science & Business Media, 2011.
8. Lang, W. *Sensors and Measurement systems*; River Publishers, 2019.
9. Inman, D.J.; Singh, R.C. *Engineering vibration*; Vol. 3, Prentice Hall Englewood Cliffs, NJ, 1994.
10. Meirovitch, L. Analytical Methods in Vibrations, McMillan Pub. Co. *Inc., New York* **1967**.
11. Weaver Jr, W.; Timoshenko, S.P.; Young, D.H. *Vibration problems in engineering*; John Wiley & Sons, 1991.
12. Haus, J.N.; Schwerter, M.; Schneider, M.; Gäding, M.; Leester-Schädel, M.; Schmid, U.; Dietzel, A. Robust Pressure Sensor in SOI Technology with Butterfly Wiring for Airfoil Integration. Sensors 2021, 21, 6140.
13. Rittmeier, L.; Roloff, T.; Haus, J.N.; Dietzel, A.; Sinapius, M. Design of a Characterisation Environment for a MEMS Ultrasound Sensor under Guided Ultrasonic Wave Excitation. Engineering Proceedings 2021, 10, 58.
14. Bornemann, S.; Lang, W. Experimental Study on Stress Impact during FML Manufacturing on the Functional Conformity of an Embeddable SHM-Sensor-Node. Engineering Proceedings 2021, 10, 72.